# Experimental Investigation of High-Flux Density Magnetic Materials for High-Current Inductors in Hybrid-Electric Vehicle DC-DC Converters

Marek S. Rylko, Member, IEEE, John G. Hayes, Member, IEEE, Michael G. Egan, Member, IEEE
University College Cork, Ireland
rylkoms@gmail.com, john.hayes@ucc.ie, m.egan@ucc.ie

***Abstract* – High-flux-density materials, such as iron-based amorphous metal and 6.5 % silicon steel for gapped inductors, and powdered alloys for gapless inductors, are very competitive for high-power-density inductors. The high-flux-density materials lead to low weight/volume solutions for high-power dc-dc converters used in hybrid-electric and electric vehicles. In this paper, the practical effects of frequency, dc bias, flux-density de-rating, the duty cycle, air-gap fringing on the core and winding, and thermal configuration based on lamination direction are investigated for iron-based amorphous metal, 6.5 % silicon steel and iron-based powdered alloy material. A 2.5 kW converter is built to verify the optimum material selection and thermal configuration. Analytical, simulation, and experimental results are presented.**

***Index Terms – Materials comparison, frequency effect, distributed gap effect, thermal configuration.***

## I. INTRODUCTION

There is a continuous demand for high-power-density magnetic designs in hard-switched dc-dc converters in the automotive, aerospace and stationary power generation industries. A compact and efficient magnetic design is critical to ensure that the overall weight and volume of hard-switched dc-dc converters is reduced [1]. As discussed in [2], several design options have an effect on the size of the inductor, e.g. frequency, number of stages and continuous vs. discontinuous conduction. An optimal choice of core dimensional ratios can also significantly reduce the size of the inductor [3], and further size reduction can be achieved by using improved cooling methods [4]. There is a wide variety of ferromagnetic materials available to the magnetic designer [5]-[12]. However, the optimum choice of magnetic material for a design is not straightforward. The operating dc current, current ripple, air gap length, number of air gaps, operating frequency, duty cycle, ambient and heat sink temperature and thermal path all have a strong influence on the inductor size in addition to cost and manufacturability. As shown in [13-16] the ideal material for the minimum size design, is with a small or distributed air gap together with high saturation flux and generally low power loss.

The second-generation hybrid-electric vehicles introduced by Toyota Motor Company in 2004 use 6.5% silicon steel for the boost inductor in the 30 kW+ dc-dc converter interfacing the NiMH battery [17]. More recent third-generation vehicles from Toyota tend to use powder core rather than silicon steel [17,18]. While both of these materials are high flux materials with saturation flux densities greater than 1 T, there are considerable differences between their structure, characteristics and performance. Amorphous metal tends to be price and parameter competitive with silicon steel and powdered iron and is typically also considered for automotive power trains.

TABLE I
MAGNETIC MATERIALS CHARACTERISTICS

| Magnetic Material Type | Amorphous | Silicon Steel | Powder Core |
|---|---|---|---|
| Manufacturer | Metglas | JFE | Chang Sung Corp. |
| Material | 2605SA1 | 10JNHF600 | Mega Flux |
| Composition | Fe-B-Si | 6.5% Fe-Si | Fe-Si |
| Bsat (T) | 1.56 | 1.88 | 1.6 |
| Rel. Permeability (100C @20kHz) | 600 | 600 | 26-90 |
| Curie temp. (ºC) | 395 | 700 | 725 |
| Cont. operating temperature (ºC) | 150* | 150* | 200 |
| Thermal cond. (W $m^{-1}$ $K^{-1}$) | 10** | 18.6** | TBD |
| Specific Heat Capacity [J/(K kg)] | 540 | 536 | TBD |
| Density [g/cm3] | 7.18 | 7.53 | 6.8 |
| Resistivity [μΩ m] | 1.37 | 0.82 | TBD |
| Lamination Thickness [mm] | 0.025 | 0.1 | bulk |
| Core Fill Factor | 0.83 | 0.9 | 1 |
| Magnetostriction [ppm] | 27 | 0.1 | TBD |
| Core Loss @0.1T, 20kHz [kW/$m^3$] | 70 | 150 | 186 |

* limited by the lamination epoxy, ** along laminations,
T – toroid, I4 – block core, TBD – to be determined

The experimental performance of iron based amorphous metal of type 2605SA1 supplied by Metglas [5] and 6.5% silicon steel of type 10JNHF600 supplied by JFE [6] for gapped cores, and gapless iron-based powder core of type Mega Flux 60 is supplied by Chang Sung Co. [11], are investigated in the low (15 kHz) to medium (30 kHz) frequency range.

These materials are characterized using a variety of tests which illustrate the impacts of frequency, ripple, dc bias and saturation,

978-1-4244-8218-4/10/$26.00 ©2010 IEEE

low-duty cycle, air-gap fringing, and thermal configuration on the inductor performance.

In general, inductor core losses are reduced with increased frequency and lower ripple. Core losses can increase due to high dc bias and low (and high) duty cycles. Earlier publications show air-gap fringing to result in significantly increased core losses [19,20]. Results presented in this paper show that air-gap fringing core losses are minor for these types of high-frequency inductors. Given the relatively high core losses in these materials, cooling is key for inductor performance. This paper shows that the thermal performance is very dependent on lamination direction for the laminated materials.

Testing in this paper tends to be based on foil windings, which tend to be significantly impacted by air-gap fringing. Silicon steel can be more easily manufactured compared to amorphous metal to include multiple air gaps to reduce air-gap fringing copper losses.

The experimental validation of the practical effects of the frequency, dc bias and flux density de-rating, asymmetrical waveforms effects, an gap effects on the core and winding, and thermal configuration are presented in Section II.

## II. Experimental Investigation

This section presents the theoretical and experimental investigation of the three high-flux materials: amorphous metal 2605SA1, silicon-steel 10JNHF600, and powdered core Mega Flux 60 shown in Fig. 1. The single-cut amorphous metal inductor is composed of two CC core halves. The silicon steel and the powder core inductors use block cores. The inductors are not the same size due to the cores availability.

### *A. Frequency Effect Analysis*

In this section, the power losses of the three high flux materials are compared for a range of flux densities and frequency.

Curves of the theoretical volumetric power loss vs. frequency are plotted in Fig. 2 for amorphous metal (2605SA1), silicon steel (10JNHF600) and powdered iron (Mega Flux 60) for three different peak flux density levels of 0.03 T, 0.1 T, and 0.3 T.

As shown in Fig. 2, the power loss relationship between amorphous metal and silicon steel remains relatively fixed across the frequency range of 10 kHz to 100 kHz and flux density change 0.03 T to 0.3 T. The Mega Flux 60 powder core displays strong variability with flux density amplitude. The Mega Flux 60 power loss is lower than amorphous metal if the flux density amplitude is below 20 mT. In the flux density amplitude range between 20 mT and 100 mT, the Mega Flux 60 power loss is between amorphous metal and silicon steel. Finally, the Mega Flux 60 generated power loss is greater than silicon steel if flux density amplitude is greater than 100 mT as shown in Fig. 2.

The various inductors were built and tested in order to validate the material losses. The inductors were tested in similar conditions with the similar flux density amplitude and dc bias in the experimental hard-switched boost converter set up. The inductors were examined with a constant inductance and varied frequency from 15 kHz to 30 kHz in steps of 5 kHz. Natural convection cooling is used and each test was run until the inductor reaches a steady state temperature.

Fig. 3. shows the theoretical and experimental core temperature rises above ambient for the iron-based amorphous metal, silicon-steel and powder core inductors. As expected, the measured and theoretical temperature rises of the cores decrease with increasing frequency. The theoretical predictions are generated by the algorithm developed in [15]. Since the same inductor is used across the frequency range (15-30 kHz), the flux density amplitude decreases as frequency increases, and the peak ac flux density and resulting core power loss decrease with frequency.

The experimental results are a good agreement with theoretical predictions, which over estimates temperature rise by up to 15 %. The amorphous metal and silicon steel inductors are operating with the same flux density amplitude while the Mega Flux 60 inductor operates with about 80 % of the flux density amplitude of the other two inductors.

As predicted, the silicon steel core has a temperature rise twice that of amorphous metal for the same excitation. The powdered core has comparable temperatures to the silicon steel but is running at lower flux than the silicon steel. As noted earlier, as the frequency increases, decreasing the flux level, the powder core loss reduces significantly.

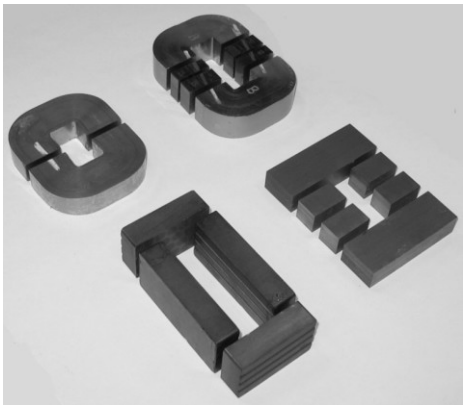

Fig. 1. Single-cut Fe-based amorphous (left), multi-cut Fe-based amorphous (top), 6.5% Si steel (right) and Fe-based powder core (bottom).

### *B. Dc-Bias Effect on the Core Power Loss*

The magnetic material permeability varies with magnetic field and it is a function of frequency, dc bias and flux density amplitude and temperature. The permeability change of the presented materials is negligible in the frequency range of interest [5-12]. The magnetic material permeability generally decreases with the applied dc-magnetizing force [5, 8, 12, 21].

The power loss generated in the core at constant flux density magnitude is not constant and depends on the dc magnetizing force applied to the core, as discussed in [22] for ferrites.

Two inductors were built and tested in order to investigate the power loss generated in the AM and SS core as function of the dc bias. The inductors, based on amorphous metal 2605SA1 and silicon steel 10JNHF600, are built without an air gap and are examined at 100 kHz operating frequency in a 1.25 kW boost converter. The high frequency provides a low current ripple resulting in a low winding ac power loss. This allows the core power loss to be the dominating source of power loss and temperature rise. The amorphous metal based inductor winding power loss is about 10 % of the total component power loss and is small in comparison to the core losses. The silicon steel based inductor winding power loss is about 25 % of total component power loss and its effect is noticeable.

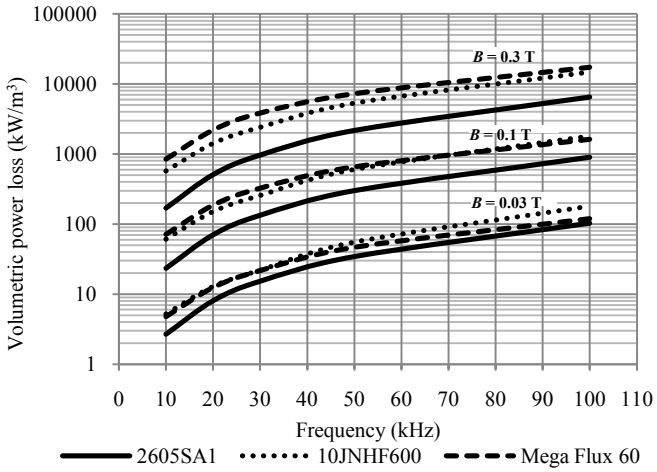


Fig. 2. Volumetric power density vs. frequency and flux density amplitude.

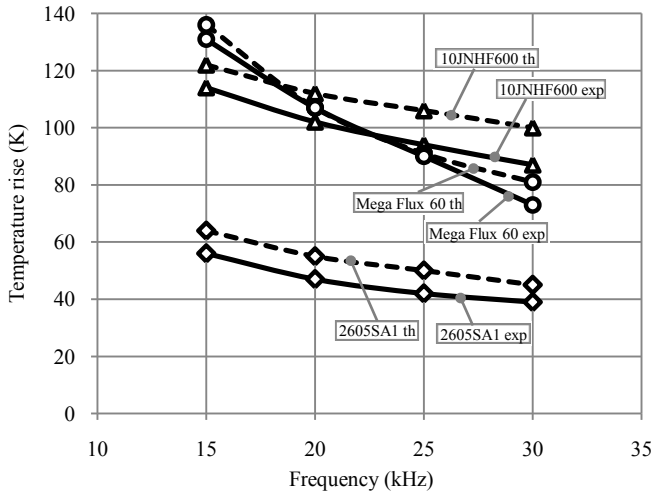


Fig. 3. Core temperature rise vs. frequency for constant inductance.

The magnetic cores are almost identical, but the amorphous metal inductor has a 30-turn winding while SS inductor has a 50-turn winding. This is due to materials' dc bias characteristics as the SS core with a 30-turn winding would not enter into deep saturation. Thus, the amorphous metal core operates at 35 mT and the silicon steel core at operates at 20 mT across the wide range of the dc magnetizing force. Natural convection cooling is used and the system is run until the inductor reaches a steady state temperature.

Fig. 4 shows the inductor temperature rise above the ambient and the theoretical B-H curve for the amorphous metal 2605SA1 inductor. As the dc magnetizing force increases, the inductor operates at elevated flux density. The measured temperature rise is nearly constant and close to the calculated temperature rise in the first region of the curve and then increases significantly as the dc bias increases beyond the knee point of about 0.6 kA/m and 1.2 T. The theoretical model clearly underestimates core power loss at elevated dc-bias.

This effect may be critical for high-current inductor where the magnetizing force applied to the core may be relatively large and inductances roll off is allowed. The power loss increase due to dc bias should be considered for the minimum size inductor design as it may be one of limiting factor in the inductor minimization.

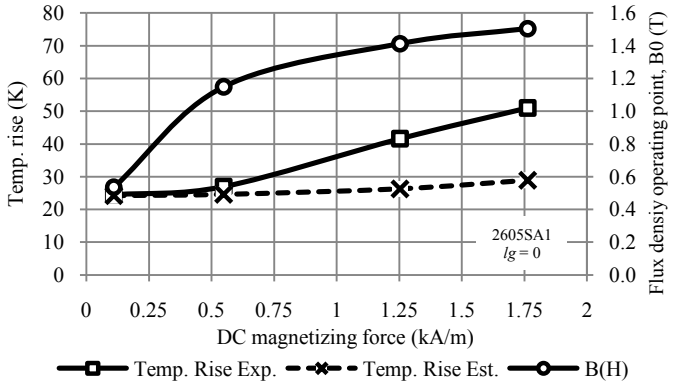


Fig. 4. 2605SA1 power loss and flux density vs. magnetizing dc-bias.

Similar behavior is observed in Fig. 5 for the silicon steel core. Due to the dc bias characteristics the SS core uses a 50-turn winding, which results in a lower flux density amplitude and higher winding power loss than for the amorphous metal inductor. Thus, the core power loss is not developed as good as for amorphous metal. However, Fig. 5 shows the general trend of the core power loss increasing at elevated dc bias. Note that silicon steel has softer dc bias characteristics than amorphous metal.

It is critical for inductor to keep its desired inductance at required operation range. As is shown in Fig. 4 and Fig. 5, operation at elevated dc bias results in increased power loss. The air gap increases the core dc bias capability at the expense of lower inductance. The gapless core contains distributed air gap, and so a discrete gap is not necessary.

As can be seen from Fig. 4, the maximum dc bias for 2605SA1 that is not causing elevated power loss is 1.2 T, and is a reasonable de-rating at about 75 % from the nominal saturation flux density of 1.56 T at 25 C 10JNHF600 has a softer magnetization curve, but also experiences core loss increases with dc bias. A 75 % de-rating for silicon steel suggests a design maximum of 1.41 T vs. the nominal saturation level of 1.88 T.

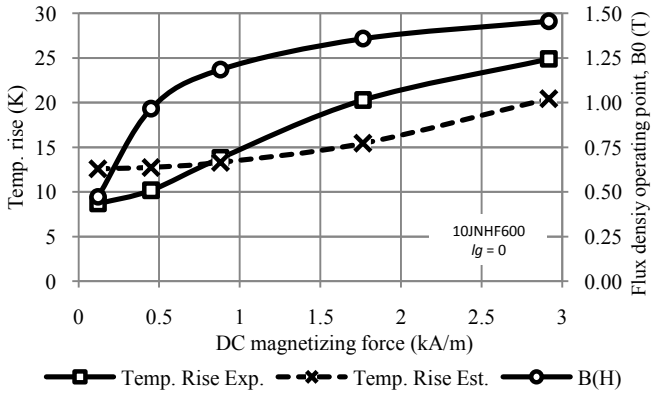


Fig. 5. 10JNHF600 power loss and flux density vs. magnetizing dc-bias.

## C. *Duty Cycle Effect on the Core Power Loss*

Switching duty cycle directly influences the volt-seconds applied to the inductor and results in magnetic flux change. The rate of change is proportional to the applied voltage. However, the same volt-seconds applied in different conditions may result in a different flux change rate. Publications based on ferrite

[23,24] show elevated power loss in the ferrite when subjected to a asymmetrical flux change patterns. Such conditions are common for boost and buck converter operation on low or high duty cycles.

There is little published on duty-cycle effects on the high-flux materials under investigation in this paper. In order to examine this effect two laminated cores and one powder core inductors were built and tested.

All cores are examined in a boost converter which operates at frequency of 10 kHz. The flux density amplitude in the core is kept constant across the duty cycle range from 0.2 to 0.5 and is 0.15 T for all inductors. The convection-cooled inductors were placed in thermal chamber and run until steady state was reached.

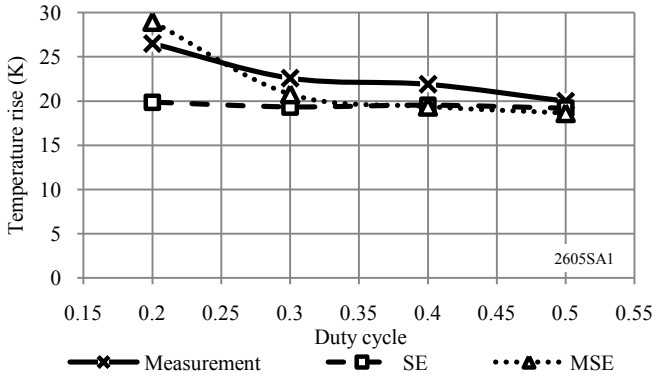


Fig. 6. Comparison between measurement and calculated temperature rise as a function of duty cycle for amorphous metal.

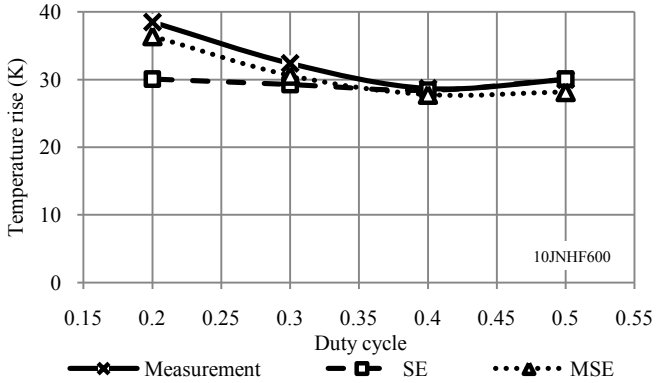


Fig. 7. Comparison between measurement and calculated temperature rise as a function of duty cycle for silicon steel.

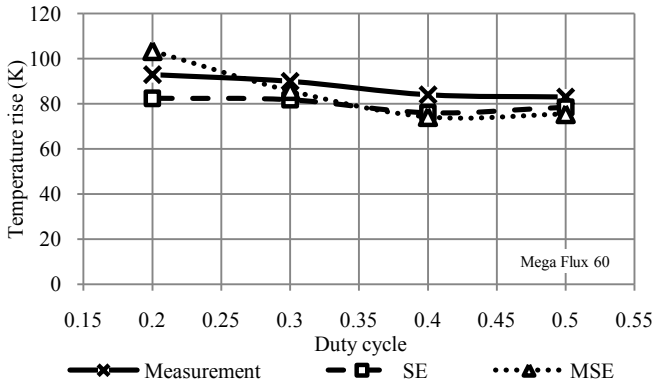


Fig. 8. Comparison between measurement and calculated temperature rise as a function of duty cycle for powder material.

The experimental temperature rise is compared with calculations, which uses inductor design flowchart presented in [15]. The Steinmetz equation, SE, model and its modified version, MSE, are used for calculation [23,24].

The experimental and predicted temperature rises using the standard Steinmetz equation and the modified version are presented for amorphous metal, silicon steel and powder core in Fig. 6, Fig. 7 and Fig. 8, respectively. It is clear that in all cases that the material core loss and temperature increase for the reduced duty cycles and that this increase is reasonably predicted by the modified Steinmetz equation.

### *D. Air Gap Effect on the Core*

In this section the power loss in the core due to air gap fringing flux is investigated.

It is reported in the literature, [19,20] and [21,24], that laminated materials can have significant additional eddy-current core loss due to the air gap fringing flux. These core losses due to the size of the air gap are caused by magnetic flux fringing around the gap re-entering the core in a direction of high loss. As the air gap increases, some of the fringing flux strikes the core perpendicular to the laminations and sets up eddy currents causing additional loss[19,20].

An experimental investigation was undertaken to define the core associated power loss due to air gap fringing flux. Two inductors were built based on the same 2605SA1 AM core as shown in Fig. 9.

One inductor has a winding placed far away from the air gap while the other inductor's winding is placed around the air gap. The inductors are examined in the dc-dc boost converter at a constant operating frequency of 50 kHz and constant flux density amplitude of 150 mT. The air gap was varied from 0 to 2 mm with 0.5 mm steps. Natural convection cooling was used and the inductors run until steady state was reached.

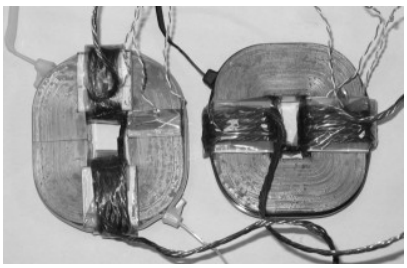

Fig. 9. Air gap experimental inductors. Winding is far away from the air gap (left), winding is shielding air gap (right).

The experimental and theoretical inductor temperature rises for the shielded and unshielded inductors are shown in Fig. 10. The temperature is largely determined by core losses as the winding losses are minimal. The unshielded experimental inductor shows a good correlation with the theoretical predictions which do not used the air gap fringing core power loss formula. If air gap fringing core power loss formula is used, then the core power loss and temperature are significantly overestimated.

The same results apply for the shielded inductor. The shielded inductor has a lower inductance and a higher current ripple with a slightly higher ac copper loss. These results show clearly that the formula presented in [19] and [20] significantly overestimates the air gap power loss in the amorphous metal core.

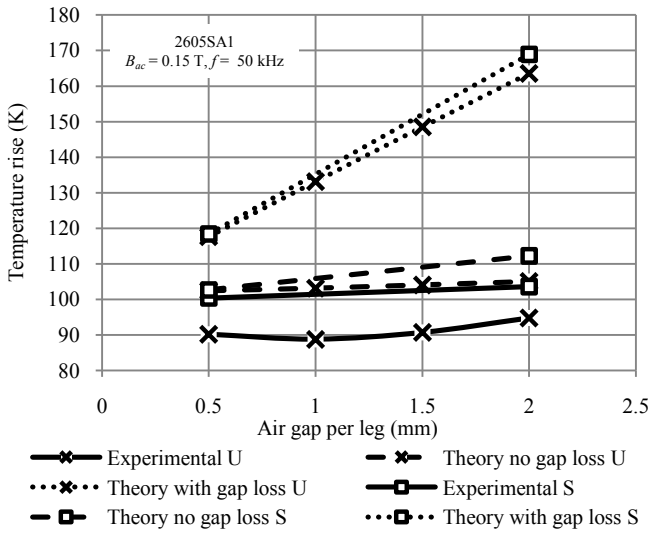


Fig. 10. Core temperature rise vs. gap length for constant frequency 50 kHz. U-winding is far away from the air gap, S-winding is shielding air gap.

The authors have continued to investigate this topic using finite element analysis. These as yet unpublished results suggest that while the air gap fringing core loss is real, the loss tends to be insignificant for these types of inductors with very thin laminations and high resistivity.

### *E. Distributed Gap Effect on Foil Winding*

In this section, the effect of the multiple gaps on the winding is investigated for amorphous metal and silicon steel.

By distributing a single gap into several smaller gaps the fringing flux is significantly reduced; thus, generated power loss. If the low permeability powder core is used an additional power loss in the winding is generated by the stray flux, which fringes outside the core. Fig. 11 shows finite element simulation results for the copper windings as a single 3 mm air gap is split into 2 gaps of 1.5 mm and 3 gaps of 1 mm respectively and the gapless powder core. As expected, the losses in the copper are decreased by distributing the air gap from approximately 16 W with a single 3 mm gap to approximately 4.5 W with three gaps of length 1 mm. The copper loss is approx. 5 W with a gapless core.

An experimental test is carried out to investigate the fringing flux effects of the distributed gap. Three cores sets are tested: three-cuts-per-leg amorphous metal and silicon steel and single-cut-per-leg amorphous metal

The total gap length per leg is 2.625 mm and the frequency is kept constant at 30 kHz. The effects of splitting this single gap into two and three smaller gaps are separately tested. For the first test, a single gap of 2.625 mm is located in the centre of the leg for the iron-based amorphous and the silicon steel cores. For the second test featuring only the multi-cut cores, there are two gaps in each leg with lengths of 1.625 mm and 1 mm respectively. The gaps are located at an equal distance from the core end sections for both materials. For the third test, again featuring only the multi-cut cores, there are three gaps in each leg with lengths of 1 mm, 1 mm, and 0.625 mm respectively. The gaps are located equally along the core leg for the iron-based amorphous core; however, the silicon steel core, because of its manufacturing process, has a 0.625 mm gap at one end of the core leg. This affects the experimental results as is discussed below.

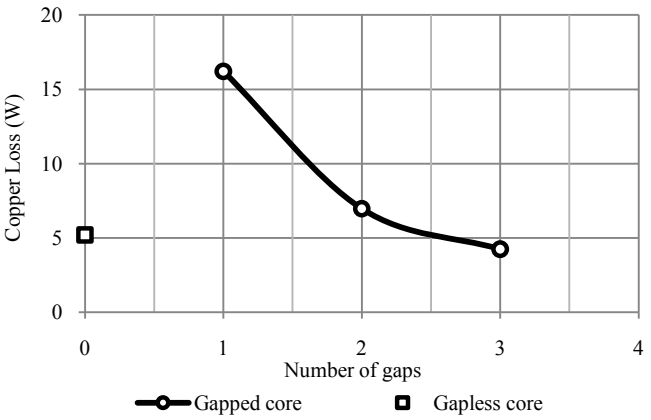


Fig. 11. FEA of distributed inductor air gap.

Fig. 12 shows the experimental temperatures decrease of the cores and the copper windings with the number of gaps for the three different core sets. As expected, the core and copper temperatures drop significantly, e.g. 18 °C for the multi-cut amorphous metal copper windings. The core for the multi-cut silicon steel only drops 7 °C because the gap located at the end of the core leg generates less winding power loss.

The single-cut amorphous metal is obviously only tested for a single gap. An interesting anomaly in this testing is that the multi-cut amorphous metal core is significantly hotter than the single-cut amorphous metal core for the single gap test point. Generally, in the testing in this paper, amorphous metal has significantly lower core loss than silicon steel. The single-cut standard amorphous metal core is operating at approx. half the temperature rise of the multi-cut amorphous metal core.

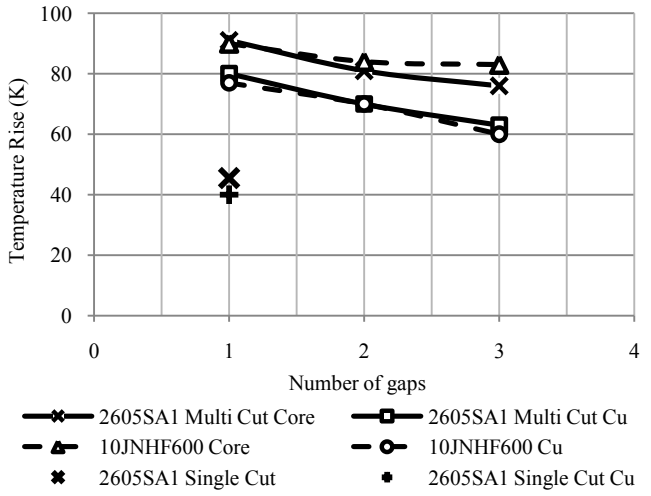


Fig. 12. Reduced core and Cu temps due to distributed gaps.

The multi-cut amorphous metal inductor tested in these experiments used a custom core with machined segments for use with the gaps. The cutting process appeared to cause shorts between the laminations and significantly increased the core heating and temperature rise as this multi-cut amorphous metal core is operating significantly hotter than predicted. In general, silicon steel is easier to generate segments and multiple cuts than amorphous metal due to the manufacturing process.

### F. Thermal Configuration

In this section the inductor core temperature rise variation with thermal conductivity and lamination direction is investigated. The temperature rise, $\Delta T$, of a material is proportional to the power loss, $P$, and thermal path, $h$, and is inversely proportional to the thermal conductivity, $\lambda$, and surface area, $A$ [25].

$$\Delta T = \frac{P\,h}{\lambda\,A} \tag{1}$$

The lamination direction has a significant impact on the thermal conductivity and subsequent heating of the inductor core. The silicon steel core is developed using a stamping process. The thermal conductivity of the material is 18.6 $W{\cdot}m^{-1}{\cdot}K^{-1}$ along the lamination [6] and approx. 1 $W{\cdot}m^{-1}{\cdot}K^{-1}$ against the lamination. The iron-based amorphous metal is developed using a winding process. The thermal conductivity of this material is 10 $W{\cdot}m^{-1}{\cdot}K^{-1}$ along the lamination and only 0.5 $W{\cdot}m^{-1}{\cdot}K^{-1}$ against the lamination [5]. The powder material is bulk and isotropic. The manufacturer is not providing thermal conductivity for Mega Flux 60; however, similar cores from Mag. Inc. are specified at 8 $W{\cdot}m^{-1}{\cdot}K^{-1}$. The lamination direction is a critical parameter regarding the inductor mounting as it affects both thermal conductivity and thermal path length. The iron-based amorphous metal must be mounted horizontally to ensure the thermal conductivity along the lamination is used. Horizontal mounting also reduces the length of thermal path for regular inductor cores. The silicon steel material should be mounted vertically to ensure thermal conduction along the lamination direction unless another cooling path is provided for the core. The vertically mounting method increases the length of thermal path for most inductor cores.

An aluminum thermal bracket shown in Fig. 13 is designed for thermal evaluation. The bracket ensures that the surface area, $A$, and thermal path, $h$, in (1) are equal for both materials. The other two parameters of (1) are dependent on the core material. The inductor cores are mounted horizontally. The aluminum bracket has a thermal conductivity of 206 $W{\cdot}m^{-1}{\cdot}K^{-1}$ [23], and extracts the heat out of the inductor core both along and against the lamination direction.

The thermal test is carried at 30 kHz. Three thermal conditions are tested. Firstly, heat is extracted from the cores optimally in the $x$-$y$ directions. The silicon steel has the lowest temperature rise due to its higher thermal conductivity. The powder material has the highest temperature rise although lowest power loss. This is influenced by lower thermal conductivity and longer core. The experimental results are shown in Fig. 14.

In the second test, heat is extracted along the $x$ direction only as a Teflon barrier is used to block heat flow in the $y$ direction. There is only a relatively small increase in temperature for the silicon steel core as the heat is still been extracted along the lamination. However, there is a larger increase in temperature for the iron-based amorphous core because the heat flow is against the lamination using the poorer thermal conductivity. The powder core temperature increases slightly as the heat exchange area decrease.

In the final test, heat is pulled out in the $y$ direction only and a Teflon barrier is used to block heat flow in the $x$ direction. This test is almost optimum for the amorphous metal but is against the lamination for silicon steel resulting in a significant temperature increase due to the poorer thermal conductivity. The powder core temperature rise is similar to $x$ direction.

In general, the experimental results correlate well with the specified thermal conductivities for the various materials and highlight the critical factor of lamination direction.

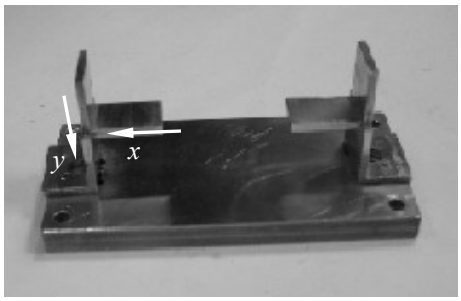


Fig. 13. Aluminum thermal jig.

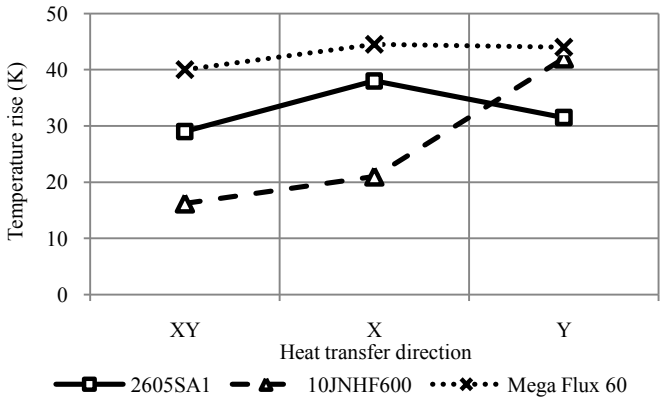


Fig. 14. Heat flow considerations.

## III. Conclusions

The iron-based amorphous metal, 6.5 % silicon steel and iron-based powder cores are competitive materials for high-power-density inductors leading to a low cost and low weight/volume solution for high-power dc-dc converters.

The practical effects of frequency, dc-bias and duty cycle on core power loss, air-gap fringing on the core and winding losses, and the lamination direction on thermal path are experimentally investigated for these materials. A 2.5 kW boost converter is built to verify the optimum material selection and thermal configuration over the frequency range and ripple ratio of interest. Experimental, analytical and simulation results are presented.

The various materials variation of core loss with frequency is approximately as predicted by the specifications. However, all materials can experience increased core losses with dc bias and appropriate de-rating should be used when operating high on the magnetization curve.

Similarly, asymmetric duty cycles result in increased core losses. The modified Steinmetz equation is a useful predictor of these increased losses.

It has been suggested in the literature that increased core loss can occur due to air gap fringing. Testing is this study suggests that these effects can be insignificant for these cores with thin laminations and high resistivity.

Finally, it is demonstrated than lamination direction is key to optimum thermal cooling path for the laminated gapped cores.

## REFERENCES


[1] Brian J. Masserant, E. William Beans, Thomas A. Stuart, "A study of volume versus frequency for soft switching IGBT converters," *IEEE Transactions on Aerospace and Electronic Systems*, Vol. 31, No. 1, January 1995, pp. 280-287.

[2] R.M. Schupbach, J.C. Balda, "35 kW ultracapacitor unit for power management of hybrid electric veicles: bi-directional dc-dc converter design," *IEEE Power Electronics Specialists Conference*, 2004, pp. 2157-2163.

[3] Robert A. Jensen, Charles R. Sullivan, "Optimal core dimensional ratios for minimizing winding loss in high frequency gapped-inductor windings," *IEEE Applied Power Electronics Conference*, 2003, pp. 1164-1169.

[4] M. Gerber, J.A. Ferreira, I.W. Hofsajer and N. Seliger, "A very high density, heatsink mounted inductor for automotive applications," *IEEE Industry Applications Conference*, 2002, pp. 948-954.

[5] www.metglas.com

[6] www.jfe-steel.co.jp

[7] www.vacuumschmelze.de

[8] www.ferroxcube.com

[9] www.micrometals.com

[10] www.mag-inc.com

[11] www.changsung.com

[12] www.arnoldmagnetics.com

[13] B.J. Lyons, J.G. Hayes, M.G. Egan, "Magnetic material comparisons for high-current inductors in low-medium frequency dc-dc converters," *IEEE Applied Power Electronics Conference*, 2007, pp. 71-77.

[14] B.J. Lyons, J.G. Hayes, M.G. Egan, "Experimental Investigation of Iron-based Amorphous Metal and 6.5% Silicon Steel for high-current inductors in low-medium frequency dc-dc Converters," *IEEE Industrial Applications Conference,* 2007, pp. - .

[15] M.S. Rylko, B.J. Lyons, K.J. Hartnett, J.G. Hayes, M.G. Egan, "Magnetic material comparisons for high-current gapped and gapless foil wound inductors in high frequency dc-dc converters," *EPE-PEMC*, 2008.

[16] M.S. Rylko, K.J. Hartnett, J.G. Hayes, M.G. Egan, "Magnetic material selection for high power high frequency inductors in dc-dc converters," *IEEE Applied Power Electronics Conference*, 2009, pp. 2043-2049

[17] N. Nozawa, T. Maekawa, S. Nozawa, K. Asakura, „Developement od power control unit for compact-class vehicle," *SAE International Journal of Passenger Cars-Electronic and Electrical Systems*, October 2009, vol. 2 no. 1, pp. 376-382.

[18] Bong-Gi You, Jong-Soo Kim, Byoung-Kuk Lee, Gwang-Bo Choi, Dong-Wook Yoo, "Optimization of powder core inductors of buck-boost converters for hybrid electric vehicles," *Vehicle Power and Propulsion Conference*, 2009, pp. 730-735.

[19] Colonel Wm. T. McLyman, *Transformer and Inductor Design Handbook*, 2nd ed., Marcel Dekker, Inc., 1988.

[20] Reuben Lee, *Electronic Transformers and Circuits*, 2nd ed., John Wiley & Sons, Inc., 1955.

[21] M. Namikawa, H. Ninomiya, T. Yamaji, "High silicon steel sheets realizing excellent high frequency reactor performance," *JFE Technical Report*, 2005.

[22] C.A. Baguley, B. Carsten, U.K. Madawala, "The effect of dc bias conditions on ferrite core losses," *IEEE Transactions on Magnetics*, Vol. 44, No. 2, February 2008, pp. 246-252

[23] Alex Van den Bossche, Vencislav Cekov Valchev, Inductors *and Transformers for Power Electronics*, CRC Press, 2005.

[24] J.Reinert, A.Brockmeyer, R.W.A.A. De Doncker, "Calculation of losses in ferro- and ferromagnetic materials based on the modified Steinmetz equation," *IEEE Transactions on Industry Applications*, Vol. 37, No. 4, July/August 2001, pp. 1055-1061.

[25] M. Gerber, J.A. Ferreira, I.W. Hofsajer and N. Seliger, "A high-density heat-sink-mounted inductor for automotive applications," *IEEE Transactions on Industrial Applications*, Vol. 40, No. 4, July/August 2004, pp. 1031-1038.

[26] J. Petzold, "Advantages of softmagnetic nanocrystaline materials for modern electronic applications," *Journal of Magnetism and Magnetic Materials*, 2002, pp. - .